




Hopping crossover and high-temperature superspin glass behavior in Ni films deposited on MoS₂

P. M. Shand ^{*}, Y. Moua, H. Harms, C. Gorgen , C. J. Cunningham, P. V. Lukashev , T. E. Kidd, and A. J. Stollenwerk
Physics Department, University of Northern Iowa, Cedar Falls, Iowa 50614-0150, USA



(Received 11 December 2023; revised 21 April 2024; accepted 11 June 2024; published 27 June 2024)

Realizing the potential of MoS₂ and other two-dimensional semiconductors in spintronic devices requires a fundamental understanding of their interaction with ferromagnetic metals. We have investigated the transport and magnetic properties of thin Ni films grown on single-crystal MoS₂ substrates. The Ni is found to have a granular morphology with an average grain size of approximately 2 nm. Like previously investigated granular Ni/insulator composites below the percolation threshold, transport is found to proceed via hopping. However, our Ni/MoS₂ sample exhibits a dual crossover: activated hopping to $T^{-1/2}$ variable-range hopping at a higher temperature and then a transition to power-law behavior at a lower temperature. The magnetoresistance was used as a novel probe for uncovering superspin-glass-like behavior above room temperature in the Ni/MoS₂ nanostructure, which also exhibits a collective ferromagnetic state at very low temperatures, reminiscent of superferromagnetism.

DOI: [10.1103/PhysRevB.109.245432](https://doi.org/10.1103/PhysRevB.109.245432)

I. INTRODUCTION

Thin ferromagnetic films have attracted the interest of researchers for many decades [1–10]. The recent discovery of ferromagnetism in monolayers of materials such as CrI₃ has significantly amplified research efforts because of interest in the fundamental physics of ferromagnetism at the two-dimensional (2D) limit and also the potential for numerous applications in the developing field of spintronics [11–14]. Because the films are atomically thin, external parameters other than a magnetic field can be used to perturb the magnetic state of the film. For example, an electric field has been used to modify the coercivity (and hence the magnetocrystalline anisotropy) of iron-based alloy films [15], while ferroelectric polarization has been predicted to have a significant impact on the magnetocrystalline anisotropy energy in cobalt and iron thin films [16,17]. In addition, magnetic proximity effects have been observed in various thin-film systems. Examples of proximity-related phenomena that have been observed include enhancement of coercivity and Curie temperature of Fe₃GeTe₂ coupled with FePS₃ [18]; tuning of valley polarization and valley Zeeman splitting in WSe₂/CrI₃ heterostructures [19]; giant proximity exchange and flat Chern band in CrB₃/MoS₂ heterostructures [20]; and spin-orbit torque switching of the magnetization in Fe₃GeTe₂/Pt bilayers [21]. This list is a small subset of the large number of tunable physical effects displayed by 2D ferromagnet-based heterostructures that are both interesting from a fundamental science perspective and potentially useful for applications in magnetoelectronic device development.

Quantum confinement effects are also an important aspect of the behavior of thin films as the 2D limit is approached [22–26]. Thin films of nonmagnetic metals (Au, Ag, and Pd)

deposited on MoS₂ exhibit quantized electronic growth modes due to periodic dips in the density of states at the Fermi level associated with certain nesting vectors of the Fermi surfaces of the metals. The weak van der Waals bonding in MoS₂ reduces the effect of strain due to lattice mismatch between the film and the MoS₂ substrate.

In view of the intriguing effects of quantum confinement and proximity described above, the deposition of a thin film of Ni on a layered van der Waals semiconductor embodies a simple system that may exhibit interesting characteristics. This system has been studied computationally via density functional theory [27]. In that work, the density of states and magnetic properties of stacks consisting of one or two monolayers of Ni and two monolayers of WSe₂ or MoS₂ were investigated. The layers were configured to minimize lattice mismatch and hence strain. It was found that the interfacial layer of the dichalcogenide became metallic, whereas the inner layer remained semiconducting. The metallization was accompanied by a modest level of spin polarization. The Ni layers remained strongly ferromagnetic but with a somewhat reduced Ni moment in the interfacial layer. Recent experimental work on thin Ni films deposited on MoS₂ showed that the Ni, which has a relatively large lattice mismatch with and binds strongly to MoS₂, tends to form clusters 1–3 nm in size distributed continuously over the film [28]. The resistance of the system increases with decreasing temperature, which indicates that electron transport is nonmetallic in nature. The system also displayed nonsaturating, linear negative magnetoresistance up to 90 kOe. The magnitude of the magnetoresistance ratio ($\sim 0.06\%/kOe$) was larger than the values for bulk Ni and granular Ni films.

In this work, we present the results of a comprehensive investigation of the magnetotransport properties of a thin Ni film deposited on MoS₂. We find that the clustered state of the Ni film leads to hopping conduction and glassy characteristics that are manifested in the magnetotransport behavior at

^{*}Contact author: paul.shand@uni.edu

temperatures above room temperature. At low temperatures, the Ni/MoS₂ system transitions to collective ferromagnetic behavior. Magnetically glassy behavior is most often probed by means of magnetization and susceptibility. We show here that magnetotransport measurements can be an effective means of shedding light on the behavior of such systems.

II. EXPERIMENTAL DETAILS

The samples were prepared by depositing Ni onto the cleaved surface of commercially available MoS₂ in a vacuum chamber with a base pressure of 5×10^{-10} mbar. Deposition occurred at room temperature using a 2 mm Ni wire (99.995% pure) in a mini electron-beam evaporator (MANTIS QUAD-EV). A flux monitor was used to maintain a consistent deposition rate calculated to be 2.5 Å/min from the resulting scanning tunneling microscopy (STM) images. Samples scanned using STM had Ni thickness ranging from a fraction of a monolayer up to 5 nm. Samples used in the resistance and magnetic measurements had a 5-nm thickness of Ni. Typical Ni grain sizes in the films were in the 1–3 nm range. After leaving the deposition chamber, the sample investigated for this work was exposed to air for 2–3 h to attach electrical leads. Gold leads were attached to the sample using silver epoxy. A Quantum Design DynaCool Physical Property Measurement System was used to perform transport measurements between 375 and 5 K. Resistance measurements were performed with a 0.5-Hz, 1 μ A driving current to minimize heating effects at low temperatures. Magnetization measurements were carried out with a Quantum Design MPMS SQUID magnetometer. The uncertainty in resistance values as measured by the standard deviation over an averaging time and repeated measurements is less than 0.1% for resistances less than 1 M Ω and less than 1% for values higher than 1 M Ω . Resistances just exceed 1 M Ω for only the lowest measurement temperature of 5 K.

III. RESULTS AND DISCUSSION

A. Film characteristics

Significant effort has been devoted to the growth of metal films on layered crystalline substrates such as graphene and transition-metal dichalcogenides [29–32]. While many metals exhibit three-dimensional (3D) island growth on graphene at room temperature (though Eu exhibits 2D growth) [29,30], layer-by-layer epitaxial room-temperature growth has been demonstrated for fcc metals on MoS₂ [31]. Ni, though fcc, was not found to grow epitaxially; it formed small, polycrystalline grains with no preferred orientation [31].

Figure 1 shows a histogram of cluster sizes in a 100 nm \times 100 nm scanning tunneling microscope image of the Ni film (shown in the inset) deposited at room temperature on MoS₂ that was used in our experiments. The size distribution is relatively narrow and centered close to 2 nm. The morphology of the film is clearly granular, with typical grain/cluster sizes of 1–3 nm. Though the individual clusters are distinct with visible boundaries, in many cases there are connections or bridges between the clusters in the distribution. The highly granular character of the Ni film on MoS₂ is unlike the growth of noble metals such as Au, which form atomically flat islands

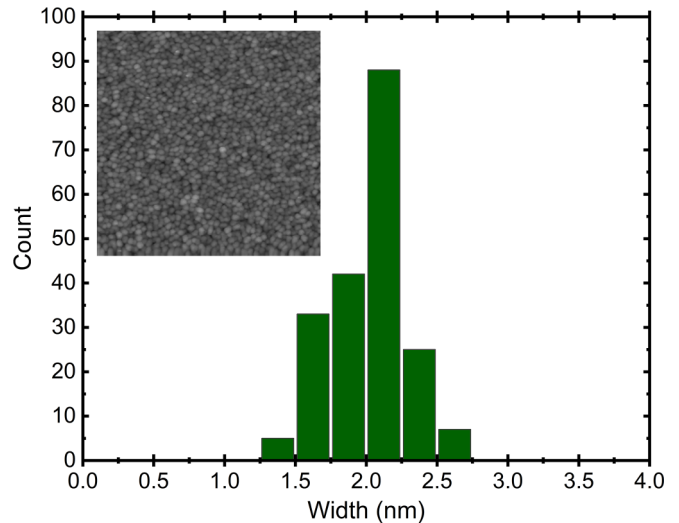


FIG. 1. Histogram of 100 nm \times 100 nm scan of clusters in the scanning tunneling microscope image of the Ni film studied in this work. The image itself is shown in the inset. The film comprises distinct grains with typical sizes ranging from 1 to 3 nm deposited on MoS₂.

on the same substrate via electronic growth. Compared to the noble metals, Ni atoms have a significantly greater binding energy on an MoS₂ surface, a larger lattice mismatch, and lower mobility. Saidi [32] has tabulated values of the ratio of the adhesive and the cohesive energy ($E_{\text{ads}}/E_{\text{coh}}$) and diffusion barriers for adatoms for many metals on MoS₂. Compared to other metals, Ni has a relatively large $E_{\text{ads}}/E_{\text{coh}}$ ratio, mainly due to its very large value of E_{ads} and moderate value of E_{coh} . Thus, Ni would tend to bind strongly to MoS₂ with little diffusion across the substrate and moderate binding to itself. This is consistent with the formation of small polycrystalline clusters as was previously mentioned and strikingly similar to the morphology of our sample. Additional details on the STM scan and the characteristics of the Ni film can be found in Ref. [28].

B. Transport in zero magnetic field

Figure 2(a) shows the logarithm of the resistance versus temperature for the Ni/MoS₂ sample. The system exhibits semiconductor-like behavior, with the resistance increasing by several orders of magnitude as the temperature decreases from 375 to 5 K. The semilog graph clearly shows that there are three distinct regions of behavior as the temperature is varied. This is more clearly demonstrated by plotting the derivative of $\ln(R)$ versus T , as shown in the inset of Fig. 2(a). To understand this behavior, we treat the Ni film as a granular metallic system with individual grains separated by a dielectric spacer of varying thickness. Strong binding of Ni to the MoS₂ single-crystal and significant lattice mismatch drive the agglomeration of the Ni into nanoclusters. The spacer is the surface layers of MoS₂. As previously noted, the as-grown films were exposed to air to prepare them for measurements, leading to the growth of an oxide layer. However, oxidation of Ni proceeds slowly [33] under ambient conditions, and any

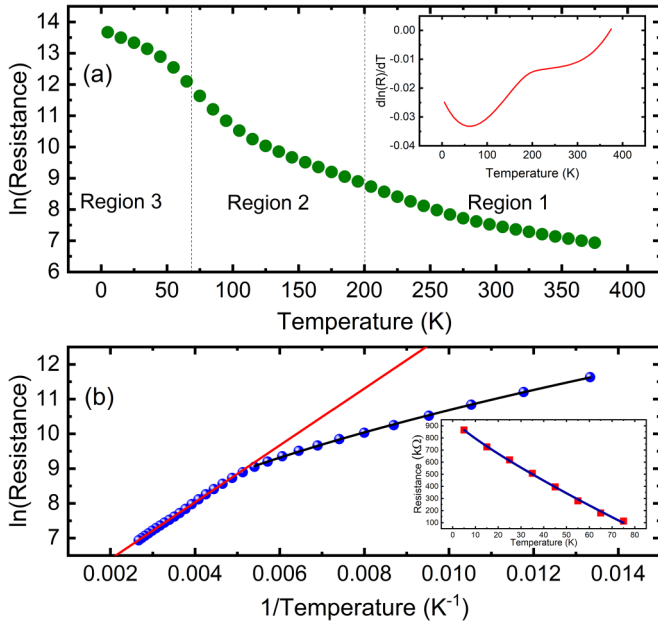


FIG. 2. (a) $\ln(\text{Resistance})$ vs temperature for Ni film on MoS_2 . The inset shows the derivative of the $\ln(R)$ vs T plot, which clearly indicates three regions of behavior. (b) $\ln(\text{Resistance})$ vs $1/T$ along with fits for activated hopping (red line, higher temperatures) and $T^{-1/2}$ variable-range hopping (black line, lower temperatures). The inset shows a power-law fit to the lowest-temperature data.

oxide layer is expected to contribute negligibly to the transport and magnetic properties.

Electric transport in granular materials has been extensively investigated over several decades [34–41]. In most cases, the systems studied experimentally consisted of metal grains dispersed within an insulating matrix. If the volume fraction of the metal exceeds the percolation threshold, the system becomes metallic. For lower volume fractions, insulating behavior ensues. The situation is, however, made more complex by a distribution of grain sizes and shapes, as well as intergrain distances. When the granular system is in the metallic phase, the resistivity typically exhibits a small positive temperature coefficient of resistance at high temperatures, which may turn negative at low temperatures due to localization effects [38,39,42]. In the insulating regime, the materials exhibit hopping behavior extending over a wide temperature range [34,38,41,43,44]. The most common variations of the resistivity as a function of temperature exhibited by granular materials are (i) purely activated (Arrhenius) behavior corresponding to nearest-neighbor (NN) hopping [42,45,46]

$$\rho = \rho_0 \exp(E_a/k_B T) \quad (1)$$

(ii) Mott variable-range hopping in three dimensions [38,41,47],

$$\rho = \rho_M \exp[(T_M/T)^{1/4}] \quad (2)$$

and (iii) Efros-Shklovskii (ES) variable-range hopping [36,44,48,49],

$$\rho = \rho_{\text{ES}} \exp[(T_{\text{ES}}/T)^{1/2}]. \quad (3)$$

In two dimensions, the exponent for the Mott law is $1/3$ [50]. The prefactors in Eqs. (2) and (3) are only weakly temperature-dependent. Figure 2(b) shows a plot of $\ln(R)$ versus $1/T$ for temperatures between 375 and 75 K. The high-temperature data (Region 1: $375 \leq T \leq 200$ K) display linear behavior, as corroborated by the excellent linear fit. This indicates that the system exhibits thermally activated NN hopping, with an activation energy $E_a = 70$ meV. This exponential dependence on $1/T$ could also be due to donor carriers freezing out in the MoS_2 substrate. We therefore tried to fit the function $R = AT^n \exp(E_d/2kT)$, where n varies with the temperature dependence of the mobility. (When $n = 3/4$, the mobility is temperature-independent.) For various values of n in the range $-1 \leq n \leq 2$, the function gave a good fit but significantly worse in quality than the pure activated behavior described by Eq. (1). We also tried a sum of the donor freeze-out and activated behavior, which gave unphysical results. Figure S1 in the supplemental material provides more details on the fitting [51]. Thus, we conclude that the granular Ni/ MoS_2 system exhibits thermally activated NN hopping behavior in the high-temperature region.

Thermally activated behavior has been predicted to occur in granular materials for temperatures for which $kT \ll E_a$, where E_a is the single-electron charging energy [45,46]. Temperatures in Region 1 of Fig. 2 are certainly well below E_a/k . If we take $E_a \sim e^2/\kappa a$, where κ is the dielectric constant ($\kappa \approx 8$ for MoS_2) and a is a characteristic length, we find that $a \approx 3$ nm. This seems reasonable given the typical cluster size of our sample.

For $200 \leq T \leq 75$ K, Fig. 2(b) shows the fit using Eq. (3), i.e., variable range-hopping accounting for charged-grain interactions. We also attempted a fit using Eq. (2)—Mott variable range hopping, for both two and three dimensions—but the fit quality was definitely lower than that for the ES $T^{-1/2}$ form. See Fig. S2 in the supplemental material for more information on the fitting [51]. The best-fit value of $T_{\text{ES}}^{1/2}$ was found to be $60.7 \text{ K}^{1/2}$. ES-type variable-range hopping has been found to describe transport over wide temperature ranges in granular metals [36,38,39,48]. For films of Ni embedded in SiO_2 , Sheng *et al.* [36] found a $T_{\text{ES}}^{1/2}$ value of $69 \text{ K}^{1/2}$ for a sample with a 44% volume fraction of Ni, which is greater than the value we obtained. Sheng *et al.* also found that the $T_{\text{ES}}^{1/2}$ value increased as the Ni volume fraction decreased, i.e., as the granular system became more insulating. Gittleman *et al.* reported that the temperature coefficient of resistivity changed from positive to negative for a Ni volume fraction below approximately 60% [34]. These findings affirm that our Ni/ MoS_2 sample is on the insulating side of a metal/insulator transition; however, just how close it is to the transition is unclear. Sheng [38] used a percolative critical path method to show that in granular materials, there is a crossover between high-temperature activated character and low-temperature Mott $T^{-1/4}$ behavior in three dimensions. The $T^{-1/2}$ behavior was hypothesized (with support from simulations) to be an interpolation between the two regimes. Experimentally, a crossover between $T^{-1/2}$ behavior at higher temperatures and $T^{-1/4}$ behavior at lower temperature has been observed in a granular metal system [41]. Further, atomically thin MoS_2 exhibits a crossover from activated to

variable-range hopping [52,53]. This behavior and that of the magnetoresistance (discussed later) point to the probed system being a composite of the Ni film and an embedding layer of MoS₂. It is worthwhile to note that the values of the prefactors obtained from the fits using Eqs. (1) and (3) are quite close; ρ_0 (in resistance units) = 117 Ω and ρ_{ES} = 100 Ω . This reinforces the conclusion that there is a crossover from activated transport to $T^{-1/2}$ variable-range hopping, given the similarity of their values. The prefactors are the “high-temperature” ($T \rightarrow \infty$) resistivities, which should be similar to classical Drude values.

There is another crossover below 70 K (Region 3) in our Ni/MoS₂ system; however, it is not to Mott variable-range hopping behavior. Instead, the resistance increase softens dramatically to a nearly linear R versus T dependence. In fact, the best fit to these data was obtained from a power law: $R = R_0 - AT^x$, with $x = 0.82$. [See the inset in Fig. 2(b).] We note that other Ni/MoS₂ samples we prepared showed the same low-temperature softening even though their resistances were up to an order of magnitude smaller at 5 K. Thus, the slope change is unlikely to be due to sample heating or instrumental issues.

Similar to our findings, Beamish *et al.* [54] discovered a crossover from $T^{-1/2}$ behavior of the resistivity to a less rapid increase at low temperatures in granular Ni/SiO₂. Chui [55] proposed an explanation based on tunneling of electrons from smaller grains to larger ones, resulting in a reduction of kinetic energy and the disappearance of the Coulomb blockade. The resulting functional form of the resistivity did not fit our lowest-temperature data. We note that the low-temperature resistivity of highly disordered 3D metals has a power-law dependence due to quantum interference-induced localization [56]. A low-temperature crossover from ordinary metallic to weak-localization behavior (accompanied by a minimum in the resistivity) due to diminished inelastic phonon scattering is often observed [57,58]. However, it seems unlikely for metallic behavior (even if highly disordered) to be found at temperatures below established hopping regimes. As mentioned above, the results suggest that both the Ni grains and MoS₂ substrate (especially within a few layers of the interface) form a composite system with distinct properties of its own. A more complex hopping mechanism similar to that suggested by Chui may be responsible for the behavior at the lowest temperatures. We note that Novosel *et al.* [43] have reported that the manganite La_{0.5}Ca_{0.5}MnO₃ undergoes a collapse of variable-range hopping at small grain sizes with a concomitant decrease in resistance and increase in the ferromagnetic contribution. This is also contrary to expectations because decreasing grain size is normally associated with increasing disorder. In this case, the system is also a composite; the grains comprise a core of antiferromagnetic/charge-ordered phase and a shell that is predominantly ferromagnetic.

Overall, the fits in all three regions are very good, though in Region 2, the difference between the Mott and ES forms is not overwhelming. Of the two Mott forms, the $T^{-1/3}$ form (corresponding to 2D systems) gives a slightly better fit. We also note that the ranges of resistance and temperature in the three regions are somewhat limited compared with those in other granular systems. Still, we are confident that the three

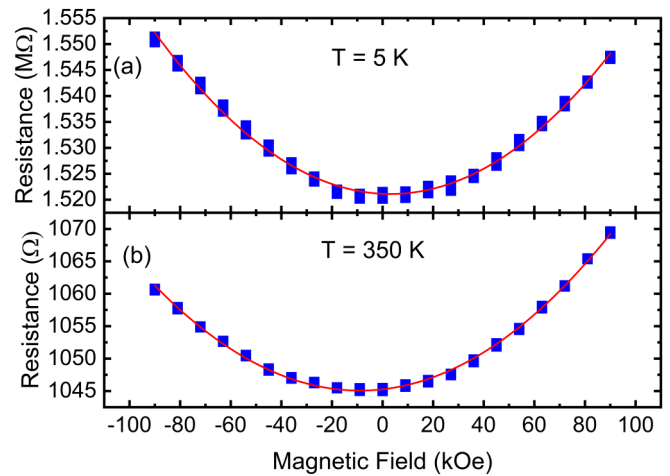


FIG. 3. (a) Resistance vs magnetic field at 5 K. (b) Resistance vs magnetic field at 350 K. The lines are second-order polynomial fits. The magnetic field is perpendicular to the plane of the film.

regimes and the quantitative descriptions we have provided appropriately capture the behavior of the composite Ni/MoS₂ system.

C. Magnetotransport

Figure 3 shows the resistance versus magnetic field for the Ni/MoS₂ sample at 5 K (a) and 350 K (b). The field is applied perpendicular to the plane of the film. The asymmetry in the latter graph is striking; there is virtually none in the former. Asymmetric magnetoresistance is typically due to switching of the magnetization at the coercive field [59] or a thickness gradient in the sample leading to the mixing of the transverse resistivity with the longitudinal resistivity [60]. However, the disappearance of the effect at 5 K indicates that these mechanisms are not the source of the asymmetry. We found that the magnetoresistance (MR) of the sample decays with time, especially at temperatures above 300 K. The timescale of the decay was comparable to that of the changes in magnetic field during the measurements, which led to the asymmetry.

The fits in both data sets are parabolas, i.e., the MR increases as H^2 . (There is a small linear term due to the asymmetry.) The MR ratio at 90 kOe is approximately 2% at both 5 and 350 K, i.e., the MR has no significant temperature dependence. This positive, quadratic MR suggests the Lorentz force, which has a B^2 dependence with no saturation for open orbits of the Fermi surface [61]. However, Lorentz magnetoresistance typically obeys Kohler’s rule, which holds that the MR ratio is inversely proportional to the square of the resistivity [62]. Thus, the MR should be smaller at lower temperatures, contrary to our results. We note that atomically thin MoS₂ exhibits a positive magnetoresistance [52]. However, in this case, the MR ratio *increases* with decreasing temperature as expected from wave-function shrinkage in a semiconductor in which localized carriers hop between defects. If both mechanisms are simultaneously present in our Ni/MoS₂ system, the countervailing temperature variations could lead to the weak temperature dependence that we observe.

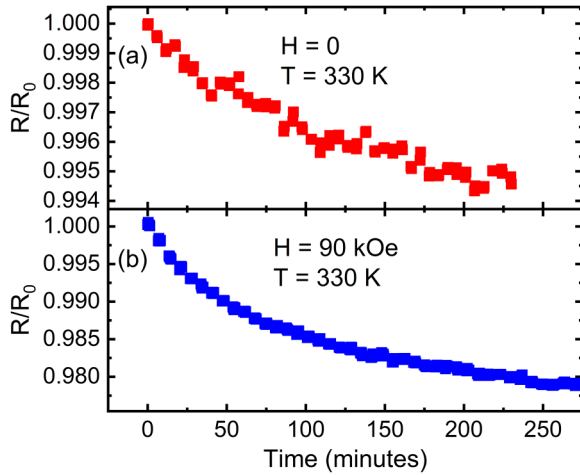


FIG. 4. (a) Normalized resistance vs time in zero magnetic field. (b) Normalized resistance vs time in a 90-kOe magnetic field. The temperature is 330 K for both measurements. The field is applied perpendicular to the plane of the film.

In many cases, ferromagnetic metal/nonmetal composites show negative MR [28,34,63]. As we will see later, the Ni/MoS₂ system studied in this work exhibits spin-glass-like behavior in magnetic fields up to 90 kOe. This suggests that the field does not have a large effect on reducing spin disorder or misalignment and thereby producing significant negative magnetoresistance.

The normalized resistance versus time at 330 K in zero magnetic field and 90 kOe is shown in Figs. 4(a) and 4(b), respectively. The resistance decays by approximately 0.5% over a 4-h period for the zero-field case. The decay is significantly stronger when the sample is subjected to a 90 kOe field at that temperature. Relaxation processes are characteristic of glassy systems such as spin glasses [64], cluster glasses [65,66], superspin glasses [67,68], and electron glasses [69,70]. The relaxation of thermodynamic variables (e.g., magnetization and susceptibility) with time is due to nonequilibrium dynamics in the glassy state. The granular nature of our Ni/MoS₂ sample brings to mind superspin glass (SSG) systems as a model for understanding its time-dependent behavior. SSG systems are typically densely packed nanoparticle systems, with each nanoparticle being a single-domain ferromagnet. The nanoparticle superspins interact via dipolar interactions, which may produce ferromagnetic or antiferromagnetic alignment depending on spatial separation. Conflicting alignments lead to frustration and glassy behavior. At low enough temperatures in a densely packed superspin system, exchange interactions can lead to a long-range-ordered superferromagnetic state [68]. SSG behavior is typically probed by magnetization and ac susceptibility measurements. Here, we have used magnetoresistance to reveal SSG-like behavior in granular Ni/MoS₂.

Figure 5 shows hysteresis measurements at 5 K (a) and 345 K (b). At 5 K, the hysteresis loop is closed with a coercivity of ~200 Oe, suggesting a collectively ordered ferromagnet. In contrast, the loop at 345 K is not closed and clearly indicates that the magnetization is drifting with time. Thus, we have strong evidence of a superferromagnetic state

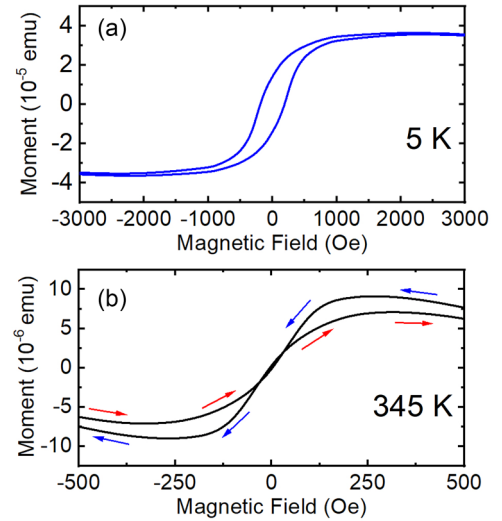


FIG. 5. (a) Hysteresis plot at 5 K. The loop is closed and there is significant coercivity. (b) Hysteresis plot at 345 K. The loop is not closed, indicating a magnetization drifting with time, i.e., relaxation is occurring.

at very low temperatures with little time dependence, which is consistent with the magnetoresistance results presented above. In addition, the relaxation of the magnetization at 345 K is in accordance with the time-dependent magnetoresistance results discussed earlier.

Figure 6 shows the decay of the resistance with time at various temperatures. All measurements were made in a 90-kOe field applied perpendicular to the plane of the film. Given that irreversibility is a typical characteristic of glassy systems, we established a protocol to ensure (to the greatest extent possible) that the state of the system was being prepared in the same manner at each temperature. The sample was cooled in a 90-kOe field to 5 K and then warmed in the same

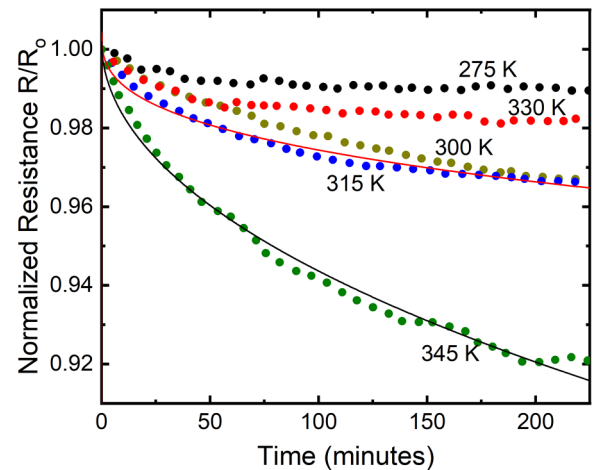


FIG. 6. Normalized resistance vs time at various temperatures. The solid lines are fits using a stretched exponential function. In each case, the sample was cooled in a 90-kOe magnetic field to 5 K and then warmed in the same field to the temperature at which the resistance relaxation measurement was performed. The field remains on during the relaxation.

field to the temperature at which the resistance relaxation measurement was performed. Figure S3 in the supplemental material has more details [51]. The relaxation rate for 345 K is much greater than the others; otherwise, there is no easily identifiable dependence of relaxation rate on temperature. This is likely due to the irreversibility mentioned above; the system is always in the glassy state. The solid lines are fits to the 345 and 315 K data with a stretched exponential $R/R_0 = A \exp[-(t/t_0)^n]$, which provides a useful mechanism for quantitatively describing relaxation processes. For $T = 315$ K, $n = 0.35$ and $t_0 = 2.18 \times 10^6$ min. For $T = 345$ K, $n = 0.5$ and $t_0 = 2.78 \times 10^4$ min. The fits show that the data generally follow the stretched exponential form. There are systematic oscillations of the data about the fits, suggesting that in addition to the overall relaxation rate indicated by the stretched exponential, there may be shorter timescale processes occurring as well.

To probe the glassy characteristics of granular Ni/MoS₂ more deeply, we carried out memory and rejuvenation measurements. Spin glasses of all types exhibit both of these properties. Consider a system in the glassy state that has been aged for a given amount of time at a certain temperature. The system will evolve towards equilibrium at that temperature during the aging period. As aging proceeds, the system becomes equilibrated over an increasing length scale. If the temperature is then decreased by a small amount, the system will start to evolve towards its new equilibrium state (rejuvenation) regardless of the aging time at the previous temperature. Rejuvenation occurs over shorter length scales, as the system keeps its memory of the larger, “frozen” equilibrated regions. Thus, when the system is reheated to the original temperature, its thermodynamic state is recaptured (on the length scale of the equilibrated regions). Recent large-scale simulations have conclusively shown that rejuvenation and memory are intimately related to the interplay among different length scales of the spin system [71,72].

Rejuvenation and memory are displayed by granular Ni/MoS₂ as shown in Fig. 7(a). Using the same protocol described above, the sample was allowed to age at 345 K, after which the temperature was reduced to 300 K. It is clear that aging restarts, as the resistance relaxes upward toward a higher equilibrium value at the lower temperature. When the temperature is returned to 345 K, the resistance resumes its original decay from a point close to its value just before the temperature decrease. See Fig. S4 in the supplemental material (which includes Refs. [73,74]) for more information [51]. Figure 7(b) shows the results of repeating the experiment but heating the sample after the initial aging rather than cooling it. It is clear that when the system is returned to the original temperature, there is no memory of the initial state. Heating destroys memory of the equilibrated regions because larger length scales (higher free-energy barriers) can be probed. Note that during the “rejuvenation” stage, the resistance time decay does not have the usual relaxation character because there is no new aging on smaller length scales. The totality of these results represents strong evidence that our granular Ni/MoS₂ sample exhibits superspin glass behavior with a possible crossover to a superferromagnetic state at low temperatures.

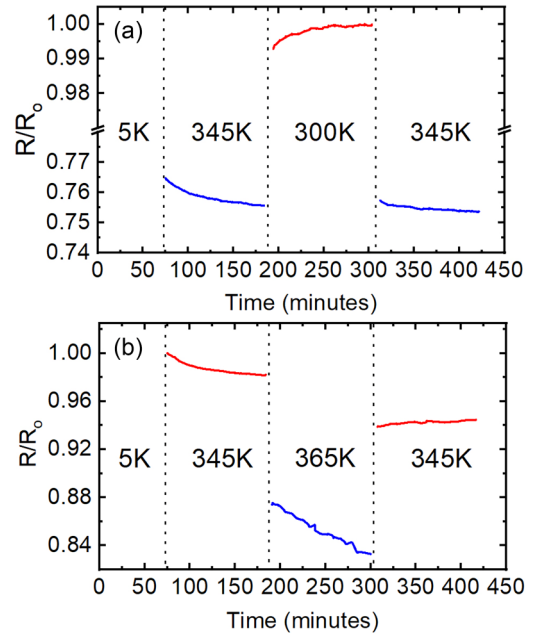


FIG. 7. (a) Aging during temperature cycling in which the temperature is first decreased and then increased back to the original value. The system displays rejuvenation at the lower temperature and then memory when the original temperature is restored. (b) Temperature cycling experiment with a positive temperature increment done first. Rejuvenation and memory are absent.

IV. CONCLUSIONS

We have experimentally investigated magnetotransport in a granular Ni film deposited on an MoS₂ single-crystal substrate. In zero magnetic field, the resistance as a function of temperature exhibits three distinct regions of behavior. In the highest-temperature region ($375 \leq T \leq 200$ K), the resistance exhibits activated (Arrhenius) behavior, characteristic of nearest-neighbor hopping. In the middle region ($200 \leq T \leq 75$ K), there is a crossover to variable-range hopping with the $\exp(AT^{-1/2})$ form, consistent with theoretical predictions for granular metals. The $\exp(AT^{-1/2})$ behavior has also been found experimentally to describe granular metals and atomically thin layers of MoS₂ over wide temperature ranges. At the lowest temperatures ($75 \leq T \leq 5$ K), the increase in resistance with decreasing temperature softens considerably, displaying power-law behavior, which does not conform with a crossover to Mott variable-range hopping $R \sim \exp(AT^{-1/4})$ at very low temperatures. The power-law behavior is reminiscent of metallic transport in disordered systems, though such a crossover to metallic behavior at low temperatures seems unlikely. We believe this behavior is a manifestation of the composite nature of the Ni/MoS₂ system. We also used the magnetoresistance as a novel probe of glassy behavior of the granular system. In zero magnetic field, the resistance decays slowly with time. When a strong magnetic field is applied, the relaxation rate increases. Magnetization measurements show collective ferromagnetic behavior at low temperatures, with little evidence of relaxation; however, at higher temperatures (near and above room temperature), an open hysteresis loop

indicates magnetization drift due to relaxation. The magnetoresistance also exhibits rejuvenation and memory, which are definitive characteristics of magnetic glassiness. We therefore identify granular Ni/MoS₂ as a superspin glass material with a possible crossover to a superferromagnetic state at low temperatures.

ACKNOWLEDGMENTS

The authors gratefully acknowledge the support of the Department of Energy, Office of Science through Grant No. DE-SC0020334. Access to a SQUID magnetometer was provided by the Nebraska Nanoscale Facility, located at the University of Nebraska-Lincoln.

- [1] R. W. Houghton, M. P. Sarachik, and J. S. Kouvel, Anomalous electrical resistivity and the existence of giant magnetic moments in Ni-Cu alloys, *Phys. Rev. Lett.* **25**, 238 (1970).
- [2] M. Rubinstein, Classical theory of giant magnetoresistance in granular metals, *Phys. Rev. B* **50**, 3830 (1994).
- [3] M. J. Aus, B. Szpunar, U. Erb, A. M. El-Sherik, G. Palumbo, and K. T. Aust, Electrical resistivity of bulk nanocrystalline nickel, *J. Appl. Phys.* **75**, 3632 (1994).
- [4] C. Chappert, D. Renard, P. Beauvillain, J. P. Renard, and J. Seiden, Ferromagnetism of very thin films of nickel and cobalt, *J. Magn. Magn. Mater.* **54**, 795 (1986).
- [5] V. A. Marsocci, Magnetoresistance and Hall-voltage measurements on single-crystal Ni and Ni-Fe thin films, *J. Appl. Phys.* **35**, 774 (1964).
- [6] A. Gerber, A. Milner, B. Groisman, M. Karpovsky, A. Gladkikh, and A. Sulpice, Magnetoresistance of granular ferromagnets, *Phys. Rev. B* **55**, 6446 (1997).
- [7] A. Frydman and R. C. Dynes, Magnetoresistance of granular ferromagnets—observation of a magnetic proximity effect? *Solid State Commun.* **110**, 485 (1999).
- [8] S. Legvold, D. T. Peterson, P. Burgardt, R. J. Hofer, B. Lundell, T. A. Vystek, and H. Gärtner, Residual resistivity and aging-clustering effects of Cu-Rich Cu-Ni alloys, *Phys. Rev. B* **9**, 2386 (1974).
- [9] S. J. Glass and M. J. Klein, Thin ferromagnetic films, *Phys. Rev.* **109**, 288 (1958).
- [10] T. T. Chen and V. A. Marsocci, Transverse magnetoresistivity anisotropy measurements and the geometrical size effect in nickel thin films, *J. Appl. Phys.* **43**, 1554 (1972).
- [11] Y. Liu and C. Petrovic, Three-dimensional magnetic critical behavior in CrI₃, *Phys. Rev. B* **97**, 014420 (2018).
- [12] A. Dimoulas, Perspectives for the growth of epitaxial 2d van der Waals layers with an emphasis on ferromagnetic metals for spintronics, *Adv. Mater. Interfaces* **9**, 2201469 (2022).
- [13] L. Chen, J.-H. Chung, T. Chen, C. Duan, A. Schneidewind, I. Radelytskyi, D. J. Voneshen, R. A. Ewings, M. B. Stone, and A. I. Kolesnikov, Magnetic anisotropy in ferromagnetic CrI₃, *Phys. Rev. B* **101**, 134418 (2020).
- [14] N. Sivadas, S. Okamoto, X. Xu, C. J. Fennie, and D. Xiao, Stacking-dependent magnetism in bilayer CrI₃, *Nano Lett.* **18**, 7658 (2018).
- [15] M. Weisheit, S. Fähler, A. Marty, Y. Souche, C. Poinsignon, and D. Givord, Electric field-induced modification of magnetism in thin-film ferromagnets, *Science* **315**, 349 (2007).
- [16] P. V. Lukashev, T. R. Paudel, J. M. Lopez-Encarnacion, S. Adenwalla, E. Y. Tsymlal, and J. P. Velev, Ferroelectric control of magnetocrystalline anisotropy at cobalt/poly (vinylidene fluoride) interfaces, *ACS Nano* **6**, 9745 (2012).
- [17] P. V. Lukashev, J. D. Burton, S. S. Jaswal, and E. Y. Tsymlal, Ferroelectric control of the magnetocrystalline anisotropy of the Fe/BaTiO₃ (001) interface, *J. Phys.: Condens. Matter* **24**, 226003 (2012).
- [18] L. Zhang, X. Huang, H. Dai, M. Wang, H. Cheng, L. Tong, Z. Li, X. Han, X. Wang, and L. Ye, Proximity-coupling-induced significant enhancement of coercive field and curie temperature in 2d van der Waals heterostructures, *Adv. Mater.* **32**, 2002032 (2020).
- [19] K. L. Seyler, D. Zhong, B. Huang, X. Linpeng, N. P. Wilson, T. Taniguchi, K. Watanabe, W. Yao, D. Xiao, and M. A. McGuire, Valley manipulation by optically tuning the magnetic proximity effect in WSe₂/CrI₃ heterostructures, *Nano Lett.* **18**, 3823 (2018).
- [20] N. Paul, Y. Zhang, and L. Fu, Giant proximity exchange and flat chern band in 2d magnet-semiconductor heterostructures, *Sci. Adv.* **9**, eabn1401 (2023).
- [21] M. Alghamdi, M. Lohmann, J. Li, P. R. Jothi, Q. Shao, M. Aldosary, T. Su, B. P. Fokwa, and J. Shi, Highly efficient spin-orbit torque and switching of layered ferromagnet Fe₃GeTe₂, *Nano Lett.* **19**, 4400 (2019).
- [22] D. K. Goswami, K. Bhattacharjee, B. Satpati, S. Roy, P. V. Satyam, and B. N. Dev, Preferential heights in the growth of Ag islands on Si (1 1 1)-(7 × 7) surfaces, *Surf. Sci.* **601**, 603 (2007).
- [23] T. E. Kidd, J. Weber, R. Holzapfel, K. Doore, and A. J. Stollenwerk, Three-dimensional quantum size effects on the growth of Au islands on MoS₂, *Appl. Phys. Lett.* **113**, 191603 (2018).
- [24] T. E. Kidd, E. O'Leary, A. Anderson, S. Scott, and A. J. Stollenwerk, Self-assembled Ag(111) nanostructures induced by Fermi surface nesting, *Phys. Rev. B* **100**, 235447 (2019).
- [25] T. E. Kidd, S. Scott, S. Roberts, R. Carlile, P. V. Lukashev, and A. J. Stollenwerk, Electronic growth of Pd (111) nanostructures on MoS₂, *J. Appl. Phys.* **129**, 174303 (2021).
- [26] T. E. Kidd, P. Kruckenberg, C. Gorgen, P. V. Lukashev, and A. J. Stollenwerk, Criteria for electronic growth of Au on layered semiconductors, *J. Appl. Phys.* **132**, 245301 (2022).
- [27] A. J. Stollenwerk, L. Stuelke, L. Margaryan, T. E. Kidd, and P. V. Lukashev, First principles study of nearly strain-free Ni/WSe₂ and Ni/MoS₂ interfaces, *J. Phys.: Condens. Matter* **33**, 425001 (2021).
- [28] T. E. Kidd, P. M. Shand, A. Stollenwerk, C. Gorgen, Y. Moua, L. Stuelke, and P. V. Lukashev, Large-field magnetoresistance of nanometer scale nickel films grown on molybdenum disulfide, *AIP Adv.* **12**, 035233 (2022).
- [29] X. Liu, C.-Z. Wang, M. Hupalo, H.-Q. Lin, K.-M. Ho, and M. C. Tringides, Metals on graphene: Interactions, growth morphology, and thermal stability, *Cryst.* **3**, 79 (2013).
- [30] D. McDougall, H. Hattab, M. T. Hershberger, M. Hupalo, M. H. von Hoegen, P. A. Thiel, and M. C. Tringides, Dy uniform film

- morphologies on graphene studied with SPA-LEED and STM, *Carbon* **108**, 283 (2016).
- [31] A. C. Domask, K. A. Cooley, B. Kabius, M. Abraham, and S. E. Mohney, Room temperature van der Waals epitaxy of metal thin films on molybdenum disulfide, *Cryst. Growth Des.* **18**, 3494 (2018).
 - [32] W. A. Saidi, Trends in the adsorption and growth morphology of metals on the MoS₂(001) surface, *Cryst. Growth Des.* **15**, 3190 (2015).
 - [33] J. G. Lisoni, L. Goux, T. Hoffmann, D. E. Diaz-Droguett, and M. Jurczak, Influence of the microstructure on the oxidation of Ni thin films, *Corros. Sci.* **59**, 282 (2012).
 - [34] J. I. Gittleman, Y. Goldstein, and S. Bozowski, Magnetic properties of granular nickel films, *Phys. Rev. B* **5**, 3609 (1972).
 - [35] J. I. Gittleman, B. Abeles, and S. Bozowski, Superparamagnetism and relaxation effects in granular Ni-SiO₂ and Ni-Al₂O₃ films, *Phys. Rev. B* **9**, 3891 (1974).
 - [36] P. Sheng, B. Abeles, and Y. Arie, Hopping conductivity in granular metals, *Phys. Rev. Lett.* **31**, 44 (1973).
 - [37] P. Sheng and J. Klafter, Hopping conductivity in granular disordered systems, *Phys. Rev. B* **27**, 2583 (1983).
 - [38] P. Sheng, Electronic transport in granular metal films, *Philos. Mag.* **B 65**, 357 (1992).
 - [39] T. Chui, G. Deutscher, P. Lindenfeld, and W. L. McLean, Conduction in granular aluminum near the metal-insulator transition, *Phys. Rev. B* **23**, 6172 (1981).
 - [40] O. Entin-Wohlman, Y. Gefen, and Y. Shapira, Variable-range hopping conductivity in granular materials, *J. Phys. C* **16**, 1161 (1983).
 - [41] S. P. McAlister, A. D. Inglis, and D. R. Kroeker, Crossover between hopping and tunnelling conduction in Au-SiO₂ films, *J. Phys. C* **17**, L751 (1984).
 - [42] I. S. Beloborodov, A. V. Lopatin, V. M. Vinokur, K. B. Efetov, Granular electronic systems, *Rev. Mod. Phys.* **79**, 469 (2007).
 - [43] N. Novosel, D. Rivas Góngora, Z. Jagličić, E. Tafra, M. Basletić, A. Hamzić, T. Klaser, Ž. Skoko, K. Salamon, and I. Kavre Piltaver, Grain-size-induced collapse of variable range hopping and promotion of ferromagnetism in manganite La_{0.5}Ca_{0.5}MnO₃, *Cryst.* **12**, 724 (2022).
 - [44] K. Yamaura, D. P. Young, and R. J. Cava, Thermally induced variable-range-hopping crossover and ferromagnetism in the layered cobalt oxide Sr₂Y_{0.5}Ca_{0.5}Co₂O₇, *Phys. Rev. B* **63**, 064401 (2001).
 - [45] K. B. Efetov and A. Tschersich, Transition from insulating to non-insulating temperature dependence of the conductivity in granular metals, *Europhys. Lett.* **59**, 114 (2002).
 - [46] I. S. Beloborodov, A. V. Lopatin, and V. M. Vinokur, Coulomb effects and hopping transport in granular metals, *Phys. Rev. B* **72**, 125121 (2005).
 - [47] H. Zhu, X. Liu, K. Ruan, and Y. Zhang, Magnetic inhomogeneity and variable-range hopping transport at temperatures above the ferromagnetic transition in La_{1.4}Sr_{1.6}Mn_{2-y}Ti_yO₇ system, *Phys. Rev. B* **65**, 104424 (2002).
 - [48] A. L. Éfros and B. I. Shklovskii, Coulomb gap and low temperature conductivity of disordered systems, *J. Phys. C* **8**, L49 (1975).
 - [49] P. Barfield, V. Tran, V. Nagarajan, M. Martinez, A. Diego, D. Bergner, A. Lanzara, J. G. Analytis, and C. Ojeda-Aristizabal, Electronic transport mechanisms in a thin crystal of the Kitaev candidate α -RuCl₃ probed through guarded high impedance measurements, *Appl. Phys. Lett.* **122**, 243102 (2023).
 - [50] N. F. Mott, Conduction in non-crystalline materials: III. Localized states in a pseudogap and near extremities of conduction and valence bands, *Philos. Mag.* **19**, 835 (1969).
 - [51] See Supplemental Material at <http://link.aps.org/supplemental/10.1103/PhysRevB.109.245432> for more information, including Refs. [73,74].
 - [52] J. Xue, S. Huang, J.-Y. Wang, and H. Q. Xu, Mott variable-range hopping transport in a MoS₂ nanoflake, *RSC Adv.* **9**, 17885 (2019).
 - [53] S. Liang *et al.*, Electrical spin injection and detection in molybdenum disulfide multilayer channel, *Nat. Commun.* **8**, 14947 (2017).
 - [54] J. R. Beamish, B. M. Patterson, and K. M. Unruh, Transport properties of granular Ni_x(SiO₂)_{100-x} thin films, *MRS Online Proc. Libr. OPL* **195**, 129 (1990).
 - [55] S. T. Chui, Disappearance of the Coulomb charging energy and low-temperature resistivity of granular metals, *Phys. Rev. B* **43**, 14274 (1991).
 - [56] P. A. Lee and T. V. Ramakrishnan, Disordered electronic systems, *Rev. Mod. Phys.* **57**, 287 (1985).
 - [57] B. K. Hazra, S. N. Kaul, S. Srinath, M. M. Raja, R. Rawat, and A. Lakhani, Evidence for the absence of electron-electron coulomb interaction quantum correction to the anomalous Hall effect in Co₂FeSi Heusler-alloy thin films, *Phys. Rev. B* **96**, 184434 (2017).
 - [58] P. M. Shand, Y. Moua, G. Baker, S. Valloppilly, P. V. Lukashev, and P. Kharel, Localization effects and anomalous hall conductivity in a disordered 3d ferromagnet, *J. Magn. Magn. Mater.* **563**, 170035 (2022).
 - [59] S. Sahoo, S. Polisetty, Y. Wang, T. Mukherjee, X. He, S. S. Jaswal, and C. Binek, Asymmetric magnetoresistance in an exchange bias Co/CoO bilayer, *J. Phys.: Condens. Matter* **24**, 096002 (2012).
 - [60] A. Segal, O. Shaya, M. Karpovski, and A. Gerber, Asymmetric field dependence of magnetoresistance in magnetic films, *Phys. Rev. B* **79**, 144434 (2009).
 - [61] J. Singleton, *Band Theory and Electronic Properties of Solids* (Oxford University Press, Oxford, 2001), Vol. 2.
 - [62] R. C. O'Handley, *Modern Magnetic Materials: Principles and Applications* (Wiley, New York, 2000).
 - [63] R. Bručas, M. Hanson, R. Gunnarsson, E. Wahlström, M. van Kampen, B. Hjörvarsson, H. Lidbaum, and K. Leifer, Magnetic and transport properties of Ni₈₁Fe₁₉/Al₂O₃ granular multilayers approaching the superparamagnetic limit, *J. Appl. Phys.* **101**, 073907 (2007).
 - [64] J. A. Mydosh, *Spin Glasses: An Experimental Introduction* (CRC Press, Boca Raton, FL, 1993).
 - [65] I. M. Siouris, S. Katsavounis, V. Kontopou, A. Hoser, and R. K. Kremer, Cluster glass transition in the ternary Dy₂AgIn₃ system determined by neutron diffraction and AC-DC magnetization measurements, *J. Magn. Magn. Mater.* **514**, 167123 (2020).
 - [66] P. M. Shand, A. L. Meyer, M. Streicher, A. Wilson, T. Rash, M. W. Roth, T. E. Kidd, and L. H. Strauss, Coulomb-driven cluster-glass behavior in Mn-Intercalated Ti_{1+y}S₂, *Phys. Rev. B* **85**, 144432 (2012).

- [67] P. E. Jönsson, H. Yoshino, H. Mamiya, and H. Takayama, Absence of strong rejuvenation in a superspin glass, *Phys. Rev. B* **71**, 104404 (2005).
- [68] W. Kleemann, O. Petravic, C. Binek, G. N. Kakazei, Y. G. Pogorelov, J. B. Sousa, S. Cardoso, and P. P. Freitas, Interacting ferromagnetic nanoparticles in discontinuous $\text{Co}_{80}\text{Fe}_{20}/\text{Al}_2\text{O}_3$ Multilayers: From superspin glass to reentrant superferromagnetism, *Phys. Rev. B* **63**, 134423 (2001).
- [69] N. Kurzweil and A. Frydman, Inverse slow relaxation in granular hopping systems, *Phys. Rev. B* **75**, 020202(R) (2007).
- [70] T. Havdala, A. Eisenbach, and A. Frydman, Ultra-Slow relaxation in discontinuous-film-based electron glasses, *Europhys. Lett.* **98**, 67006 (2012).
- [71] M. Baity-Jesi, E. Calore, A. Cruz, L. A. Fernandez, J. M. Gil-Narvion, I. Gonzalez-Adalid Pemartin, A. Gordillo-Guerrero, D. Iñiguez, A. Maiorano, and E. Marinari, Memory and rejuvenation effects in spin glasses are governed by more than one length scale, *Nat. Phys.* **19**, 978 (2023).
- [72] M. Baity-Jesi, E. Calore, A. Cruz, L. A. Fernandez, J. M. Gil-Narvion, I. Gonzalez-Adalid Pemartin, A. Gordillo-Guerrero, D. Iñiguez, A. Maiorano, and E. Marinari, Temperature Chaos is present in off-equilibrium spin-glass dynamics, *Commun. Phys.* **4**, 74 (2021).
- [73] A. G. Schins, A. F. M. Arts, H. W. de Wijn, L. Leylekian, E. Vincent, C. Paulsen, and J. Hammann, Nonstationary dynamics in a two-dimensional spin glass, *J. Appl. Phys.* **69**, 5237 (1991).
- [74] E. Vincent, V. Dupuis, M. Alba, J. Hammann, and J.-P. Bouchaud, Aging phenomena in spin-glass and ferromagnetic phases: Domain growth and wall dynamics, *Europhys. Lett.* **50**, 674 (2000).